Extreme Mechanics Letters 43 (2021) 101141

Contents lists available at ScienceDirect

Extreme Mechanics Letters

journal homepage: www.elsevier.com/locate/eml

Structural strength scaling law for fracture of plastic-hardening metals and testing of fracture properties

Hoang T. Nguyen [a], A. Abdullah Dönmez [b,a], Zdeněk P. Bažant [a,*,1]

[a] Northwestern University, 2145 Sheridan Road, Evanston, IL 60208, United States of America
[b] Istanbul Technical University, Turkey

ARTICLE INFO

Article history:
Received 19 October 2020
Received in revised form 30 November 2020
Accepted 3 December 2020
Available online xxxx

In honor of Horacio Espinosa, SES Prager Medalist

Keywords:
Plastic-hardening metals
Small-scale yielding fracture
Ductile fracture
Failure load scaling
Size effect on structure strength
Asymptotic matching
Fracture energy release
Energy dissipation
J-integral
Testing of aluminum

ABSTRACT

The small-scale yielding fracture of plastic-hardening metals is a well-understood theory, essentially conceived by Hutchinson, Rice and Rosengren (hence the name HRR theory). However, even though specimens of rather different sizes have been tested to verify the small-scale yielding theory, an analytical scaling law for the size effect transition from elastic–plastic behavior through small- and large-scale yielding to fracture process zone has apparently not been formulated. Such a scaling law would be useful for the design as well as measurement of mode-I ductile fracture properties of metals, and is the aim of this study. Unlike the fracture of quasibrittle materials such as concrete or composites, the modeling of plastic-hardening materials is complicated by a millimeter scale singular yielding zone that forms between the micrometer-scale fracture process zone (FPZ) and the elastic (unloading) material on the outside. Essential for the large-scale transitional size effect is the effective yielding zone size, which is here calculated from the equivalence of the virtual works within the plastic-hardening zone and elastic singular stress fields within the transition zone, and is shown to depend on the crack-parallel T-stress. The size effect analysis requires taking into account not only the dissipation in the FPZ delivered by the J-integral flux of energy through the yielding zone, but also the energies released from the structure and from the unloaded band of plasticized material trailing the advancing yielding zone. Equating the rates of energy releases and energy dissipation leads to an approximate energetic size effect (scaling) law that matches the calculated small- and large-size asymptotic behaviors, when the crack ligament contains the yielding zone.. The law is similar to that for quasibrittle fracture but its coefficients depend on the fracture energy and the yielding zone size in a different way. This law, reducible to linear regression, can be exploited for size effect testing of fracture energy (or critical J-integral) and effective size r_p of the yielding zone. An effect of high crack-parallel stress T on r_p is likely but is relegated to future study, as it would not affect the scaling law derived. For testing of the transition from the small-size range (large-scale yielding) to the large-size range (small-scale yielding), a modified size effect method, requiring nonlinear optimization, is developed. The size effect law is verified by scaled tests of notched specimens of aluminum.

1. Introduction

The theory of small-scale yielding in fracture of plastic-hardening metals is by now a well-developed classical subject. Nevertheless, the analytical laws governing its scaling properties have apparently not been formulated, although they may be useful for fracture testing and for predicting structure strength. Their formulation is the main goal of this study.

The foundation of the small-scale yielding fracture mechanics was laid down by Hutchinson [1] and Rice and Rosengren [2]. They calculated the near-tip singular field, generally called the HRR field, in which the strain energy density exhibits a $1/r$ singularity (r = radial distance from crack tip). Essential for this advance was Rice's J-integral [3], which allowed calculating the energy flux into the crack tip under the hypothesis of negligible elastic strains and no unloading in the near-tip yielding zone. A critical value of the J-integral, J_{cr}, thus became the criterion of crack propagation, and an effective method of measuring J_{cr} was developed [3–5].

What distinguishes metals most from quasibrittle materials, such as concrete, rocks, tough ceramics and fiber composites, is that the fracture process zone (FPZ), which is of micrometer-scale width and length, is surrounded by a plastically hardening zone. In this respect, though not in others, the fracture of plastic-hardening materials is more complicated than it is for quasibrittle

* Corresponding author.
E-mail address: z-bazant@northwestern.edu (Z.P. Bažant).

[1] McCormick Institute Professor and W.P. Murphy Professor of Civil and Mechanical Engineering and Materials Science.

https://doi.org/10.1016/j.eml.2020.101141
2352-4316/

materials, in which the FPZ borders directly on an elastically unloading material.

In fracture of quasibrittle materials, the scaling, particularly the energetic size effect on the strength of specimens or structures, proved to be an essential property, not only for structural design but also for the testing of material fracture properties, including both the material fracture energy, G_f, and the characteristic FPZ size, c_f. Strangely, though, for ductile fracture of plastic-hardening metals, the problem of an asymptotically matched size effect law for the strength of geometrically similar cracked specimens or structures and for identification of material fracture properties has apparently not been studied.

Important studies of the size and behavior of the yielding zone in ductile fracture have nevertheless been contributed, and supported by extensive finite element analyses. In particular, O'Dowd and Shih [6,7] proposed the concept of J-Q-annulus surrounding the crack tip, in which the J-integral characterizes the remote stress field corresponding to a $-1/2$-power stress singularity, while Q corresponds to the second, non-singular, term of the near-tip asymptotic expansion, which represents a uniform stress field of crack-parallel T-stress. This stress was shown to act as a crack tip constraint, suppressing cleavage. The J-Q concept, however, has not been extended to a simple analytical scaling law which is the objective here. Similar comments apply to the studies of Betegón and Hancock [8], Xia, Wang and Shih [9], and Gao, Shih, Tvergaard and Needleman [10]. Although the T-stress will not affect the form of the scaling law derived here, it will affect the prediction of the effective size, r_p, of the yielding zone, which figures as a parameter in this law, identifiable by size effect tests.

The effect of crack-parallel stresses on r_p is relegated to a subsequent study. So is the likely effect of T-stress on the G_f and on the transverse width of the (micrometer-scale) fracture process zone in metals. Such effects have recently been demonstrated for quasibrittle materials [11,12].

Finally, it should be noted that, in the field of metals, the term "size effect", has been applied to a variety of different phenomena. E.g., the well-known Hall–Petch effect [13–15] is not a size effect on structure strength but the effect of grain-size on the yield strength of metal, explained by dislocation arrest at grain boundaries. In crystal plasticity, the term is used for the strength variation of miniaturized single-crystal specimens [16]. The term has also been used for the effect of geometrically necessary dislocations and of strain gradients on the yielding strength of metals. Further the term has been used for the increase of specific cutting force with a decreasing depth of a cut [17].

Another point needs to be clarified. In quasibrittle fracture, two types of size effect on structure strength [18] must nowadays be distinguished. Here we deal only with Type 2, which occurs when geometrically similar structures of different sizes contain at maximum load large similar cracks or notches. Type 1, to which most of the present analysis does not apply, occurs for failures at fracture initiation from a smooth surface, and has, for large structures, a strong statistical component.

The present objective is to find the law governing the size effect in metallic structures with large cracks propagating in the opening mode, i.e., mode I.

2. Scaling of near-tip field and of structure strength in absence of a characteristic length

Assuming homogeneous plasticity, the field of any continuum variable close enough to a perfectly sharp tip of a crack (or notch) possesses no characteristic length. Therefore, the field must be self-similar in the radial polar coordinate r centered at the tip. In other words, any response $f(r,\theta)$, such as the displacement or stress, must be such that, for any two radii r and ξr, the scaling ratio $f(\xi r,\theta)/f(r,\theta) = \rho$ would be independent of the polar angle θ. Hence, function $f(r,\theta)$ must satisfy the functional equation:

$$f(\xi r,\theta) = \rho(\xi) f(r,\theta) \tag{1}$$

To solve it, note that it will be true for all r if and only if it is true for every interval $(r, r+\mathrm{d}r)$. So we differentiate Eq. (1) with respect to ξ and get

$$r f_{,\xi r}(\xi r,\theta) = \rho'(\xi) f(r,\theta) \tag{2}$$

where $f_{,\xi r}$ and ρ' denote the derivatives on ξr and ξ. Now we may consider $\xi \to 1$ and denote $\rho'(1) = m$ = constant. This converts the functional equation into a differential equation which can be solved by separation of variables:

$$r\,\frac{\mathrm{d}f(r,\theta)}{\mathrm{d}r} = m f(r,\theta) \tag{3}$$

Its solution is $\ln f(r,\theta) = m \ln r + \ln \psi(\theta)$ where $\ln \psi(\theta)$ = integration constant independent of r but dependent on θ. So we conclude that the near-tip field must be a power law in r:

$$f(r,\theta) = r^m \psi(\theta) \tag{4}$$

Substitution into the field equation yields an eigenvalue problem in θ with an infinite series of eigenvalues m. The eigenfield of the lowest eigenvalue dominates near the tip.

Based on Eq. (4), we conclude that any field variable near the tip of a crack (as well as or V-notch) must have a separated form in polar coordinates, and that the radial dependence must be a *power function* (this conclusion also applies to various singularities in hydrodynamics, electromagnetism, electrostatics, etc.).

As a particular case, the foregoing argument applies to the nominal strength, σ_N, of geometrically similar structures with similar cracks and loadings but different characteristic sizes D (see Eq. 1–3 in [19] or Eqs. 1.2–1.4 in [20]); σ_N is a load parameter with the dimension of stress, defined as $\sigma_N = P/bD$ where P = load and b = thickness of two-dimensional (2D) structure. The conclusion is that, in absence of characteristic structure size D_0, which is the case for linear elastic fracture mechanics (LEFM), σ_N must scale as a power law of D multiplied by some constant c_S that depends only on the shape (or geometry) of the structure with crack:

$$\sigma_N = c_S D^m \tag{5}$$

3. Review of power-law stress–strain relation for plastic-hardening metals

According to the deformation theory of plasticity, it has generally been assumed that plastic-hardening metals can be adequately described by the Ramberg–Osgood [21] uniaxial stress–strain law:

$$\frac{\epsilon}{\epsilon_y} = \frac{\sigma}{\sigma_y} + \alpha_p \left(\frac{\sigma}{\sigma_y}\right)^n \tag{6}$$

where n = plastic hardening exponent; σ_y = yield strength, ϵ_y = yield strain limit; α_p = empirical parameter (usually denoted as α, but α is generally used for dimensionless crack length); and n = plastic hardening exponent, typically 3 to 20 [1,2]. Note that the material is considered plastically incompressible by volume, which means that the material yields only in shear, which allows us to deal only with deviatoric stress and strain tensors s_{ij} and e_{ij}.

Beginning with the HRR (Hutchinson–Rice–Rosengren [1,2]) theory, the elastic strain is neglected, which has the advantage that stress–strain relation becomes a power law:

$$\frac{\epsilon}{\epsilon_y} = \alpha_p \left(\frac{\sigma}{\sigma_y}\right)^n \tag{7}$$

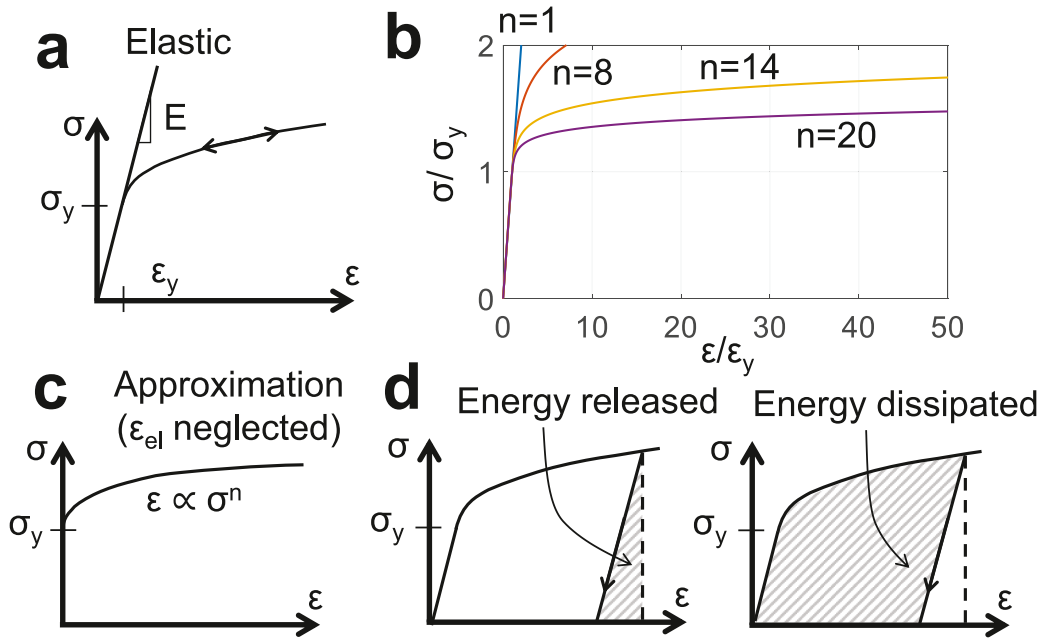

Fig. 1. (a) Stress–strain behavior of the deformation theory of plasticity (nonlinear elasticity); (b) Elasto-plastic constitutive law with different n; (c) Approximation of total stress–strain relation by plastic stress–strain relation (elastic strain is neglected); and (d) Partition of strain energy at unloading into released and dissipated.

The power law is assumed to start at 0, which ignores the initial elastic response. The benefit stemming from a power law is that it enables an analytical solution [1,2]. As shown in Fig. 1, for high exponents n, the initial plastic deformations are negligible, and σ_y represents only an equivalent yield limit characterizing the point where the power law takes off.

The simplest and apparently quite realistic tensorial generalization is [1,2,4,5]:

$$e_{ij} = \frac{3\alpha_p \epsilon_y}{2\sigma_y}\left(\frac{\sigma_{ef}}{\sigma_y}\right)^{n-1} s_{ij} \tag{8}$$

where $\sigma_{ef} = \sqrt{\frac{3}{2}s_{kl}s_{kl}}$ (9)

σ_{ef} = scalar effective stress, of von Mises type (conceivable higher-order terms such as $\sigma_{ef}^3 \propto s_{km}s_{mn}s_{nk}$ are omitted). The numerical subscripts refer to Cartesian coordinates (x_1, x_2) and the summation rule applies. Note that the use of the deformation theory of plasticity in the HRR theory is a simplifying hypothesis. Yet, it is acceptable if no unloading occurs, and is shown by Hutchinson and Paris [22] to be quite accurate.

4. Large-scale yielding in small structures

First we consider the case of large-scale yielding, in which the specimen or structure is so small that all of the fracture cross section is plastically yielding and full development of the yielding zone is prevented by the cross section size. We consider geometrically similar specimens of various sizes D, with similar cracks or notches. Based on the preceding arguments (Eq. (4)), the absence of any characteristic length implies the near-tip stress field to have a separated form:

$$s_{ij} = \sigma_y (r/r_p)^m \psi_{ij}(\theta) \tag{10}$$

where functions ψ_{ij} cannot be expressed by an exact explicit form but can be approximated by several methods, e.g. finite difference method [23,24], complex solution via conformal mapping [25,26], and finite element method [27]. It is dimensionless and thus σ_y is required for dimensional consistency. Exponent m is a constant to be determined later, and r_p represents the effective size (or radius) of the yielding zone. Substitution (10) into the constitutive law, Eq. (8), furnishes:

$$e_{ij} = \alpha_p \epsilon_y (r/r_p)^{mn} \varphi_{ij}(\theta) \tag{11}$$

where $\varphi_{ij}(\theta) = \frac{3}{2}\psi_{ij}(\theta)\left(\frac{3}{2}\psi_{kl}(\theta)\psi_{kl}(\theta)\right)^{\frac{n-1}{2}}$ (12)

where φ_{ij} are also dimensionless functions. Since e_{ij} is expressed in terms of the gradient of displacement u_i, and since an integration increases the r-exponent by 1, the displacement field must have the separated form:

$$u_i = \alpha_p \epsilon_y r_p (r/r_p)^{mn+1} F_i(\theta) \tag{13}$$

where F_i are dimensionless functions. Evaluating the expression $\epsilon_{ij} = e_{ij} = \frac{1}{2}(u_{i,j} + u_{j,i})$, we can check that it agrees with Eq. (11). At the same time, we get an expression for function $F_i(\theta)$ in terms of $\varphi_{ij}(\theta)$ (the subscripts preceded by a comma denote derivatives).

It is now useful to recall Rice's J-integral [3] giving the energy flux through the yielding zone into the fracture process zone:

$$J = \int_\Gamma \left(\bar{W}\mathrm{d}y - \nu_j s_{ij} u_{i,1}\mathrm{d}s\right), \quad \bar{W} = \int s_{ij}\mathrm{d}\epsilon_{ij} \tag{14}$$

where the flux is meant with respect to crack length a, not time; Γ is a closed contour around the crack tip, s is the length coordinate of that contour, ν_i its unit outward normal, $y = x_2$, $\partial_1 = \partial/\partial x_1$, $\frac{1}{2}s_{ij}e_{ij}$ is the stored strain energy recoverable upon unloading and $\bar{W}$ is the nonlinear strain energy density. The material is considered as nonlinearly elastic, as if the unloading would follow the same curve as loading. This hypothesis is acceptable if the J contour avoids the zone of unloading in the wake of the advancing yielding zone. Elasticity, whether linear or nonlinear, is essential for the path independence of J-integral.

Consider now the J-integral for a circular path, for which $\mathrm{d}s = r\mathrm{d}\theta$ and $\mathrm{d}y = r\mathrm{d}\theta\cos\theta$. From this and from Eqs. (18)–(20)) it follows that the radial dependence of the first term of J-integral is

$$\int_{-\pi}^{\pi} \bar{W}\mathrm{d}y \;\propto\; r^m r^{mn} r = r^{m(n+1)+1} \tag{15}$$

($\propto$ is the proportionality sign). The same must occur for the second term of J integral. Indeed,

$$\int_{-\pi}^{\pi} v_j s_{ij} u_{i,1} \mathrm{d}s \;\propto\; r^m r^{mn+1} r^{-1} r = r^{m(n+1)+1}. \tag{16}$$

(as confirmed by the complete expression in Appendix A). Since the J-integral is path independent, the exponent of r must be zero, i.e., $m(n+1)+1=0$, or

$$\boxed{m = -\frac{1}{n+1}} \tag{17}$$

as noted in 1968 by Hutchinson [1] and Rice and Rosengren [2]. As a check, for the case of a linear elastic behavior, $n=1$, and Eq. (16) gives $m=-1/2$. As another check, $s_{ij}e_{ij}$ is known [1,2] to be proportional to $1/r$ when the crack tip is approached, and this is obviously also satisfied. It should be noted that the power-law hardening is not realistic when $n>20$ [2] and, for non-hardening plastic materials $-1/(n+1)\to 0$ (or $n\to\infty$), a different solution is required [28]. In practice, though, $n\le 20$ suffices for most situations.

According to Eq. (17), Eqs. (10)–(13) for large-scale yielding in small structures now take the following particular form (same as Eqs. 5.3.10 in [5]):

$$s_{ij} = \sigma_y \left(\frac{r}{r_p}\right)^{-\frac{1}{n+1}} \psi_{ij}(\theta) \tag{18}$$

$$e_{ij} = \alpha_p \epsilon_y \left(\frac{r}{r_p}\right)^{-\frac{n}{n+1}} \varphi_{ij}(\theta) \tag{19}$$

$$u_i = \alpha_p \epsilon_y r_p \left(\frac{r}{r_p}\right)^{\frac{1}{n+1}} F_i(\theta) \tag{20}$$

The structure strength is normally characterized in terms of the nominal strength of structure, defined as $\sigma_N = P/bD$, where P is the applied load or load resultant, b is the structure width (for a two dimensional structure or specimen), and D is the characteristic structure size, measured homologously on geometrically similar structures of different sizes. Thus σ_N is a load parameter with the dimension of stress. Obviously $\sigma_N \propto s_{ij}$ and $r\propto D$, considering small enough structures with large-scale yielding, in which the plastic yielding zone occupies the entire fracture cross section. Eq. (18) thus yields the size effect law (or scaling law):

$$\boxed{\sigma_N \;\propto\; \sigma_y \left(\frac{r_p}{D}\right)^{\frac{1}{n+1}}} \quad \text{(for large-scale yielding, small } D\text{)} \tag{21}$$

where proportionality constants irrelevant to size effect are omitted. Note that, in the limit of $n\to 1$, this scaling law reduces to $\sigma_N \propto D^{-1/2}$, which is the case of linear elasticity (or LEFM) except that the material stiffness approaches zero. Although specimens or structures small enough to undergo large-scale yielding may be too small for current practical interest, Eq. (21) is nonetheless useful for anchoring the asymptotic matching of the small-to-large-scale yielding transition, which we pursue later.

5. For comparison—derivation of scaling law for quasibrittle structures with no plasticity

To derive the scaling law for small-to-large structure transition, we will need to generalize and reinterpret the approach used for quasibrittle materials [19,20,29–32], and so we review it first. We begin by the expression for energy release rate in linear elastic fracture mechanics (LEFM): $\mathcal{G} = (\sigma_N^2/E')Dg(\alpha)$ where $\alpha = a/D$, a = crack or notch length, D = characteristic structure size, and $g(\alpha) = K_I^2/(D\sigma_N^2)$ = dimensionless energy release function of LEFM reflecting the structure shape (K_I = mode I stress intensity factor, $E'=E$ for plane stress or $E/(1-\nu^2)$ for plane strain, E = Young's modulus, ν = Poisson ratio). Replacing the crack length a with the effective crack length $a = a_0 + c_f$ where c_f is a material property characterizing the effective length of the FPZ, we have $\mathcal{G} = (\sigma_N^2/E')Dg(\alpha_0 + c_f/D)$ where $\alpha_0 = a_0/D$ and a_0 = length of the stress-free crack (or notch). Taking the first two terms of the Taylor series expansion, and denoting $g_0 = g(\alpha_0)$ and $g_0' = \mathrm{d}g(\alpha_0)/\mathrm{d}\alpha$, we get $\mathcal{G} = (\sigma_N^2/E')D(g_0 + g_0'(c_f/D))$, or

$$\mathcal{G} = \mathcal{G}_s + \mathcal{G}_b \tag{22}$$

where

$$\mathcal{G}_s = (\sigma_N^2/E')Dg_0 \tag{23}$$

$$\mathcal{G}_b = (\sigma_N^2/E')c_f g_0' \tag{24}$$

where $g_0 = g(\alpha_0)$, $g_0' = [\mathrm{d}g(\alpha)/\mathrm{d}\alpha]_{\alpha_0}$. Setting $\mathcal{G} = G_f$ (material fracture energy), and solving for σ_N, we obtain, after rearrangements, the classical size effect law [29–31] (of Type 2) for geometrically similar quasibrittle structures with similar cracks or notches:

$$\sigma_N = \sqrt{\frac{E'G_f}{g_0'c_f + g_0 D}} = \frac{\sigma_0}{\sqrt{1+D/D_0}} \tag{25}$$

in which $D_0 = (g_0'/g_0)c_f$ (transitional size), $\sigma_0 = (E'G_f/c_f g_0')^{1/2}$ (this law now underlies the ACI standard code provisions for scaling of strength of concrete structures; the material characteristic length, c_f, of concrete has been shown to be about $0.4l_0$, where $l_0 = E'G_f/\sigma_y^2$ = Irwin's characteristic length [33,34]).

For test data fitting, it is useful that Eq. (25) can be rearranged to linear regression plot

$$Y = AX + C \quad \text{where} \quad X = D, \quad Y = \frac{1}{\sigma_N^2} \tag{26}$$

$$A = \frac{1}{\sigma_0^2 D_0}, \quad C = \frac{1}{\sigma_0^2} \tag{27}$$

Obtaining A and C by regression of test data, we can calculate D_0 and σ_0 and then G_f and c_f from the last equation. This method of measurement of materials fracture characteristics has become widely used for concrete and geomaterials and has been embodied in the international standard recommendation of RILEM [35] (recently also endorsed by the ACI-446 Committee). Eqs. (25)–(27) apply even when the structures or cracks for different sizes D are not geometrically similar, but function $g(\alpha)$ is then different for each size.

6. Yielding zone size under crack-parallel stress via energy matching of singular fields

Before studying the size effect, we also need an estimate of the effective size of the yielding zone, which we approximate as a circle of radius r_p. Furthermore, we must include the dependence of r_p on the crack-parallel stress $\sigma_{11} = T$ (in the case of plane stress), which represents the second term in the LEFM near-tip asymptotic series expansion. The first two terms of this expansion read [36]:

$$\sigma_{11} = \frac{K_I}{\sqrt{r}} f_{11}(\theta) + T \tag{28}$$

where $f_{11}(\theta) = \cos\theta'(1-\sin\theta'\sin 3\theta')/2\pi$, $\theta' = \theta/2$ (e.g. p. 86 in [32]), and $K_I = \sqrt{E'G_f}$ = mode I stress intensity factor of the elastic field. The T-field in the second term is nonsingular and uniform. In small-scale yielding, the σ_{ij} field in Eq. (28) prevails at sufficient distance from the yielding zone (YZ). At closer range its interference with the plastic-hardening singular near-tip field given by Eq. (10) is complicated, and requires elasto-plastic finite element analysis (the typical contour of small-scale yielding zone

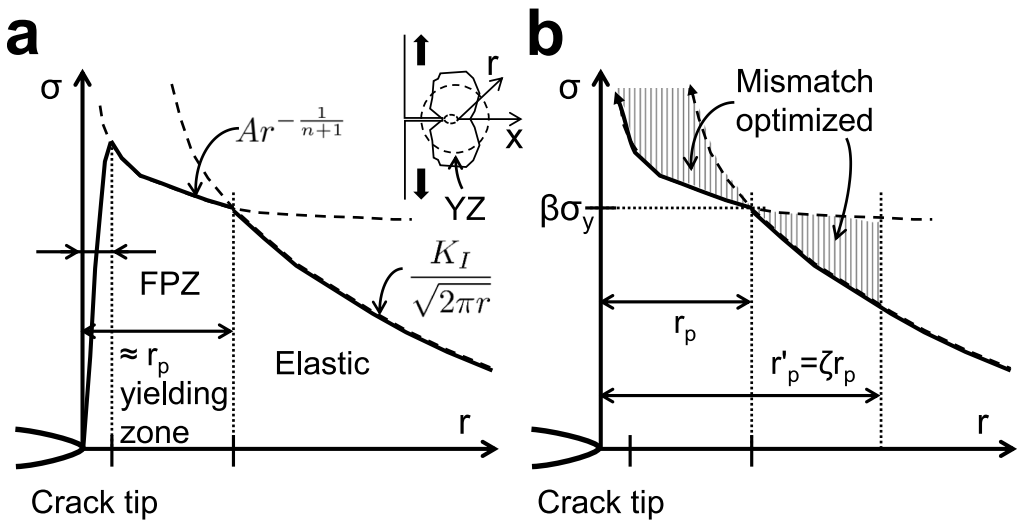

Fig. 2. Schematic radial stress profiles; (a) intersection of yielding and elastic zones; and (b) mismatch areas (cross-hatched) for equilibrium matching of both zones by virtual work.

for plane stress, obtained by finite elements [1], is shown in Fig. 3).

As a simplification, the boundary between these two fields could be estimated by the intersection of radial profiles at which the stresses from both fields are equal (as suggested by Hutchinson and Rice, and previously for perfect plasticity by Irwin). But this would still be complicated, giving r_p as a function of θ and T. Such a complication, though, is unnecessary for the global behavior such as the failure load and size effect. Besides, a dependence or r_p on θ would prevent us getting a clear result for the size effect.

In this light, we try (similar to [5]) to determine one effective constant value of transition radius r_p. To this end, we introduce a different approach—the use of the variational principle of virtual work to enforce global equilibrium, or overall energy equivalence, of the two interfering fields, Eqs. (18) and (28). With r_p defined as a constant, the stress at the intersection of the fields given by these two equations would, of course, not be equal to σ_y at each ray θ. The yield stress, σ_y, would be matched only in the average sense for all θ, and based on equilibrium in the crack direction (see Fig. 2).

Since T works on crack-parallel strain $\epsilon_{xx} = \epsilon_{11}$ in the case of plane stress, we match the two singular fields by imposing, for a circle of a certain larger radius r'_p ($> r_p$, to be estimated later), the virtual work condition of overall equivalence of the stress resultants in crack direction x_1:

$$\int_{-\pi}^{\pi}\int_{0}^{r'_p}(\sigma_{11}-T)\,r\,\mathrm{d}\theta\,\mathrm{d}r\;\delta\epsilon_{11}=\int_{-\pi}^{\pi}\int_{0}^{r'_p}\hat{s}_{11}\,r\,\mathrm{d}\theta\,\mathrm{d}r\;\delta\epsilon_{11} \tag{29}$$

$$\text{where}\quad \hat{s}_{11}=K_I\,r^{-\frac{1}{2}}f_{11}(\theta) \tag{30}$$

In the yielding zone, σ_{11} can be represented by s_{11} and expressed according to Eq. (18). Integrating, and noting that the resulting equation must be valid for any variation, we set the multiplier of $\delta\epsilon_{11}$ to zero. This gives:

$$\frac{r'_p}{\zeta}=\boxed{r_p=\frac{C_e^2 l_0}{\zeta\,(C_nC_p-\pi T/\sigma_y)^2}} \tag{31}$$

$$\text{where}\quad C_n=\zeta^{-\frac{1}{n+1}}\frac{n+1}{2n+1},\quad l_0=\frac{E'G_f}{\sigma_y^2} \tag{32}$$

$$C_e=\frac{2}{3}\int_{-\pi}^{\pi}f_{11}(\theta)\,\mathrm{d}\theta,\quad C_p=\int_{-\pi}^{\pi}\psi_{11}(\theta)\,\mathrm{d}\theta \tag{33}$$

Note that, for $T = 0$, the proportionality to l_0 is the same as in Eq. (5.4–10) of [5] but dimensionless factors C_n, C_e, C_p are different.

To estimate factor ζ, we must give equal weights to the mismatches in the yielding and elastic zones. So we require that a half of the matching zone would lie within the yielding zone and the other half in the elastic zone, i.e., $\pi r_p'^2 = 2\pi r_p^2$. This yields $r'_p \approx r_p\sqrt{2}$. However, because of the approximate nature of energy matching, the factors C_e, C_p may best be determined by FEM or experiment. See Appendix II for generalized methods to estimate r_p and r'_p (note that, for the special case of $T = 0$, another estimate of r_p was obtained in a different way in 1976 by Shih and Hutchinson [37]; they used the J-integral and superposed the displacements for the plastic-hardening and linear elasticity).

In addition to r_p, the effect of T will probably also change the energy dissipation in the FPZ, represented by J_{cr} (or G_f), as confirmed for quasibrittle materials by the gap test [11,12]. This is a separate question, which will be addressed theoretically and experimentally in a subsequent study.

Alternatively, Eq. (31) for r'_p can be obtained by least-square optimization of the matching of both singular fields, i.e., by minimizing the square of the difference between the two integrands in Eq. (29), integrated over the area of circle of radius r'_p. The minimizing condition based on the squares of the differences of stress resultant differences in the x_1 direction then is:

$$\frac{\mathrm{d}}{\mathrm{d}r'_p}\int_{-\pi}^{\pi}\int_{0}^{r'_p}\left[\sigma_{11}-T-\hat{s}_{11}\right]^2\,r\,\mathrm{d}\theta\,\mathrm{d}r\;=\;0 \tag{34}$$

7. Energy dissipation rates of small-scale yielding in large structures

Having reviewed the theory of fracture of plastic-hardening metals, we can now embark on a study of scaling. We will need the strain energy density $\bar{W}$ of the nonlinearly elastic material approximating the plastic-hardening metal. It is defined as

$$\bar{W}=\int s_{ij}\mathrm{d}e_{ij} \tag{35}$$

To calculate it, we multiply the right-hand side of Eq. (18) for s_{ij} by loading parameter μ and readily find that the right-hand side of Eq. (11) must then be multiplied by μ^n, and the expression for

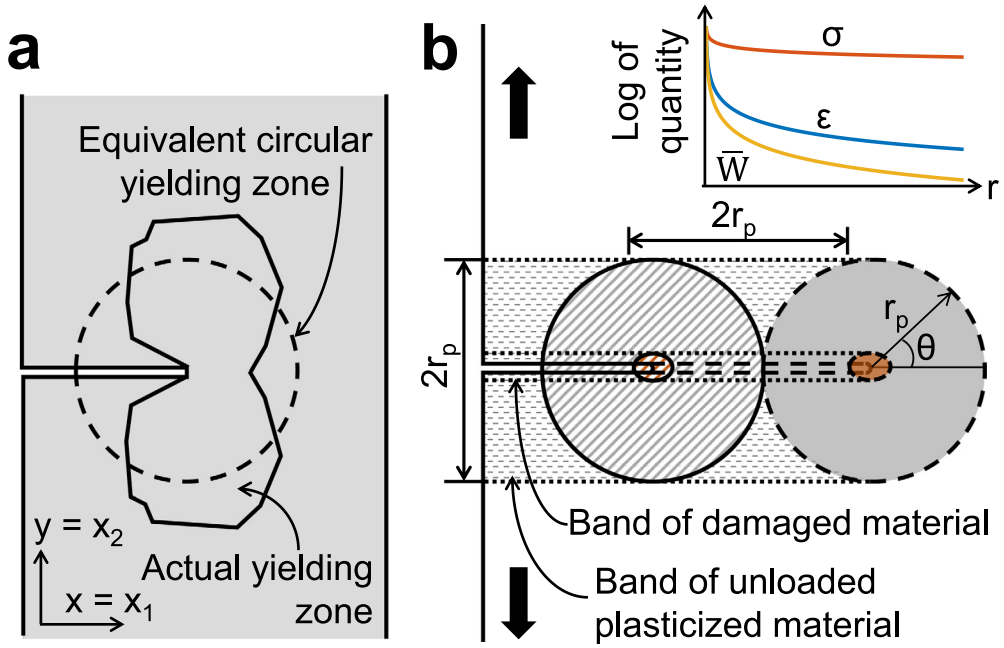

Fig. 3. (a) Actual and equivalent yielding zones with the same area (or volume), as indicated by FE analysis using von-Mises type plastic-hardening constitutive law; (b) Propagation of the equivalent yielding zone as crack grows.

de_{ij} by $n\mu^{n-1}$. Integrating from $\mu = 0$ to $\mu = 1$, we obtain the energy density

$$\bar{W}(r,\theta) = \frac{n}{n+1}\,\alpha_p \sigma_y \epsilon_y \,\frac{r_p}{r}\,\varphi_{ij}(\theta)\psi_{ij}(\theta) \tag{36}$$

Note that here and further we must use the effective radius r_p of the yielding zone instead of the radius r_p' of the larger energy matching zone. Evaluating $\int\int$[Eq. (36)] $r\,\mathrm{d}\theta\,\mathrm{d}r$, one finds that the total strain energy in the circle of radius r_p (per unit width in the transverse direction x_3) is:

$$W = \frac{n}{n+1}\,\alpha_p \sigma_y \epsilon_y r_p^2 \int_{-\pi}^{\pi} \varphi_{ij}(\theta)\psi_{ij}(\theta)\mathrm{d}\theta \tag{37}$$

After the entire yielding zone advances beyond a given point, the material gets unloaded. Although the unloaded elastic strain energy $\bar{W}_e$ may be small and negligible, it is easy to include it in our calculations. Considering only the deviatoric stresses and strains, the elastic energy density is $s_{ij}s_{ij}/2G$. Since the elastic shear modulus $G = \sigma_y/\epsilon_y$, substitution of Eq. (10) shows that the strain energy density at point (r,θ) of the yielding zone is:

$$\bar{W}_e(r,\theta) = \tfrac{1}{2}\sigma_y \epsilon_y (r_p/r)^{2/(n+1)} \psi_{ij}(\theta)\psi_{ij}(\theta) \tag{38}$$

To obtain the strain energy release rate, $\mathcal{G}_b$, due to unloading of the entire yielding zone, the strain energy contained in this zone must be divided by the distance of travel to the next non-overlapping position of the zone (Fig. 3), which is the distance $2r_p$, equal to the diameter of the yielding zone approximated as circular. So,

$$G_e = \frac{1}{2r_p}\int_{-\pi}^{\pi}\int_0^{r_p} \bar{W}_e(r,\theta)r\,\mathrm{d}\theta\,\mathrm{d}r = r_p\,\sigma_y\epsilon_y\,Q_e \tag{39}$$

$$Q_e = \frac{n+1}{8n}\int_{-\pi}^{\pi} \psi_{ij}(\theta)\psi_{ij}(\theta)\,\mathrm{d}\theta \tag{40}$$

After the passage of the yielding zone through a fixed station, the irreversible work of plastic yielding does not flow into the crack tip but is dissipated by unloading of the plasticized material. Over the effective width, $2r_p$, of the yielding zone, the energy dissipation rate is

$$G_p = \frac{1}{2r_p}\int_{-\pi}^{\pi}\int_0^{r_p} [\bar{W}(r,\theta) - \bar{W}_e(r,\theta)]r\,\mathrm{d}\theta\,\mathrm{d}r = \sigma_y\epsilon_y\,r_p\,(Q_p - Q_e) \tag{41}$$

where $$Q_p = \frac{n\alpha_p}{2(n+1)}\int_{-\pi}^{\pi}\varphi_{ij}(\theta)\psi_{ij}(\theta)\mathrm{d}\theta \tag{42}$$

8. Size effect on fracture strength of plastic-hardening structures

To exploit an analogy with the size effect mechanism in quasibrittle structures, we need to interpret Eqs. (22)–(24) physically. The energy release rates $\mathcal{G}_s$ and $\mathcal{G}_b$ correspond to two different zones in the structure: (i) $\mathcal{G}_s$ is the energy release from the undamaged, elastic, zone of the structure, which is proportional to D (approximately, though for $D \to \infty$ exactly), and (ii) $\mathcal{G}_b$ is the rate of energy release from the damage band, which is independent of D (the rates are considered with respect to crack length a, not time). This band is the zone trailed by the advancing FPZ of finite width $2r_p$ if the yielding zone is approximated as circular. Before fracture, the material in this band is under transverse tension proportional to σ_N.

Compared to quasibrittle materials, which are incapable of plastic yielding, the situation in metals is complicated by the presence of a plastic-hardening yielding zone, inserted between the damage zone and the elastic zone. The yielding zone (typically of millimeter dimensions) plays a triple role—first, it conveys energy flux J through the yielding zone to the FPZ (typically of micrometer dimensions) and, second, it also dissipates energy, at the rate G_p, as the plastically deformed material unloads in the wake of the yielding zone. However, aside from these two dissipation roles, there is a third role: as the yielding zone travels forward, it unloads, at the rate $\mathcal{G}_b$, the strain energy $(\gamma_c\sigma_N)^2/2E'$ initially stored in the band of width $2r_p$ trailed by the yielding zone (here γ_c is a certain stress concentration factor, which is independent of structure size D and which we absorb into the definition of σ_N).

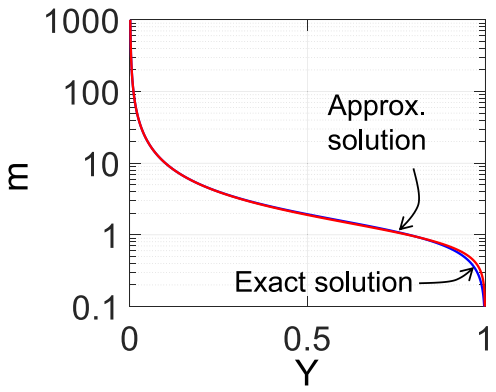

Fig. 4. Comparison of accuracy of Eq. (63) in approximating the exact solution, Eq. (62).

The rates of energy release from the elastic part of the structure and from the band swept by the yielding zone must be equal to the rates of energy dissipation at the crack tip and in the trail of the advancing yielding zone, Therefore,

$$\boxed{\mathcal{G}_s + \mathcal{G}_b = G_f + G_p} \tag{43}$$

For $\mathcal{G}_b$ we can take the same expression as in Eq. (24) but with the damage band width, c_f, replaced by $2r_p$, i.e.,

$$\mathcal{G}_b = (\sigma_N^2/E')\,2r_p \tag{44}$$

For $\mathcal{G}_s$ we can co-opt Eq. (23) (this is a simplification which may be supported by the thermodynamic theory of material (or configurational) forces used by Herrmann et al. [38,39] who observed, on that basis, that the crack widening gives approximately the same LEFM energy release rate as the crack extension; see Fig. 12.8 in [40] and [34] where this concept was refined and calibrated). Substitutions of Eqs. (23), (41), and (44) into (43) then yield the energy balance equation:

$$\frac{\sigma_N^2}{E'} D g_0 + \frac{\sigma_N^2}{E'} 2r_p = G_f + G_p \tag{45}$$

Solving for σ_N finally furnishes the size effect law:

$$\boxed{\sigma_N = \frac{\sigma_0}{\sqrt{1 + D/D_0}}} \tag{46}$$

This law has the same form as the size effect law, SEL, for quasibrittle materials (Eq. (25)) but its coefficients are expressed differently and depend on the hardening exponent n:

$$D_0 = \frac{2r_p}{g_0}, \quad \sigma_0^2 = \frac{E' G_f}{2r_p} + \sigma_p^2, \tag{47}$$

$$\sigma_p^2 = \frac{E' \sigma_y \epsilon_y}{2}\left(Q_p - Q_e\right) \tag{48}$$

The asymptotes of size effect are also of the same type:

$$\sigma_N \underset{D\to 0}{\Rightarrow} \sigma_0 = \text{constant}, \quad \sigma_N \underset{D\to\infty}{\Rightarrow} D^{-1/2} \tag{49}$$

9. Size effect method for testing material fracture properties in large enough structures in small-scale yielding range

Like Eq. (25), Eq. (46) can again be transformed to linear regression

$$\boxed{Y = AX + C} \quad \text{where} \quad X = D, \quad Y = 1/\sigma_N^2 \tag{50}$$

$$A = 1/\sigma_0^2 D_0, \quad C = 1/\sigma_0^2 \tag{51}$$

If σ_N-values are measured for various D, and σ_y, ϵ_y, α_p, E', n, and if functions $\varphi_{ij}(\theta)$, $\psi_{ij}(\theta)$ are all known, at least numerically, and if their integrals in Q_p and Q_e are evaluated (which could be done once for all), then the fracture energy G_f (equal to J_{cr}) and the effective width $2r_p$ of the yielding zone can be identified by testing the size effect. To this end, one must first determine the value of g_0 (and E'). Then one conducts linear regression of the measured data pairs (X, Y) according to Eq. (50), to get A and C, and calculates: $\sigma_0 = 1/\sqrt{C}$ and $D_0 = C/A$. Finally, if the smallest tested specimen is large enough to be in the small-scale yielding range, we have

$$r_p = \frac{g_0}{2\sigma_0^2 A}, \quad G_f = \frac{2r_p}{E'}\left(\frac{1}{\sqrt{C}} - \sigma_p\right) \tag{52}$$

10. Simple asymptotic matching of small-to-large-scale yielding

The small-size asymptote of Eq. (46), i.e. σ_N = constant, does not match the small-size large-scale yielding $\sigma_N \propto D^{-1/(n+1)}$ in Eq. (17) or (21). This is caused by considering, in our analysis, a different physical mechanism which is inappropriate for the range of transition from large-scale yielding to small-scale yielding. As the simplest, phenomenological, way to make the small-size asymptote match the power law $D^{-1/(n+1)}$ instead of D^0 without spoiling the large-size asymptote $D^{-1/2}$, Eq. (46) may be modified as follows:

$$\boxed{\sigma_N = \sigma_0 \left(\frac{D}{D_0}\right)^{-\frac{1}{n+1}} \left(1 + \frac{D}{D_0}\right)^{-\frac{n-1}{2n+2}}} \tag{53}$$

$$\text{or} \quad \sigma_N = \sigma_0 \left(\frac{D_0}{D}\right)^{\frac{1}{2}} \left(1 + \frac{D_0}{D}\right)^{-\frac{n-1}{2n+2}} \tag{54}$$

This asymptotic matching formula cannot be derived by the previous asymptotic argument, and so it cannot be used for small specimens for which D is not much larger than r_p. This is not surprising because the derivation was purely phenomenological as it was not anchored in the rate of energy release from unloading of the material swept by the advancing yielding zone. We try to remedy it next.

11. Small-to-large-scale asymptotic matching anchored in yielding zone

When the specimen or structure cross section, of size D, is smaller than the width, i.e, $D < 2r_p$, of the fully developed yielding zone, Eq. (31), we have large-scale yielding, for which we must consider the restricted yielding zone width, which we denote as $2r = h_0 D$ where h_0 is a dimensionless constant. Similar to the argument for Eq. (21), we recognize proportionality to σ_N by replacing again s_{ij} in Eq. (18) with σ_N, but replace now $2r$ with the restricted width $h_0 D$. This yields $\sigma_N = \sigma_0 (2r_p/h_0 D)^{\frac{1}{n+1}}$, from which

$$2r_p = (\sigma_N/\sigma_0)^{n+1} h_0 D \tag{55}$$

The linear elastic strain energy that was initially stored in the material and was subsequently released by the passage of the yielding zone is, per unit length in the x direction, $\mathcal{G}_b = (\sigma_N^2/E')(2r_p)$. Replacing $2r_p$ in Eq. (55), we obtain

$$\mathcal{G}_b = \frac{\sigma_0^2}{E'}\left(\frac{\sigma_N}{\sigma_0}\right)^{n+1} h_0 D \tag{56}$$

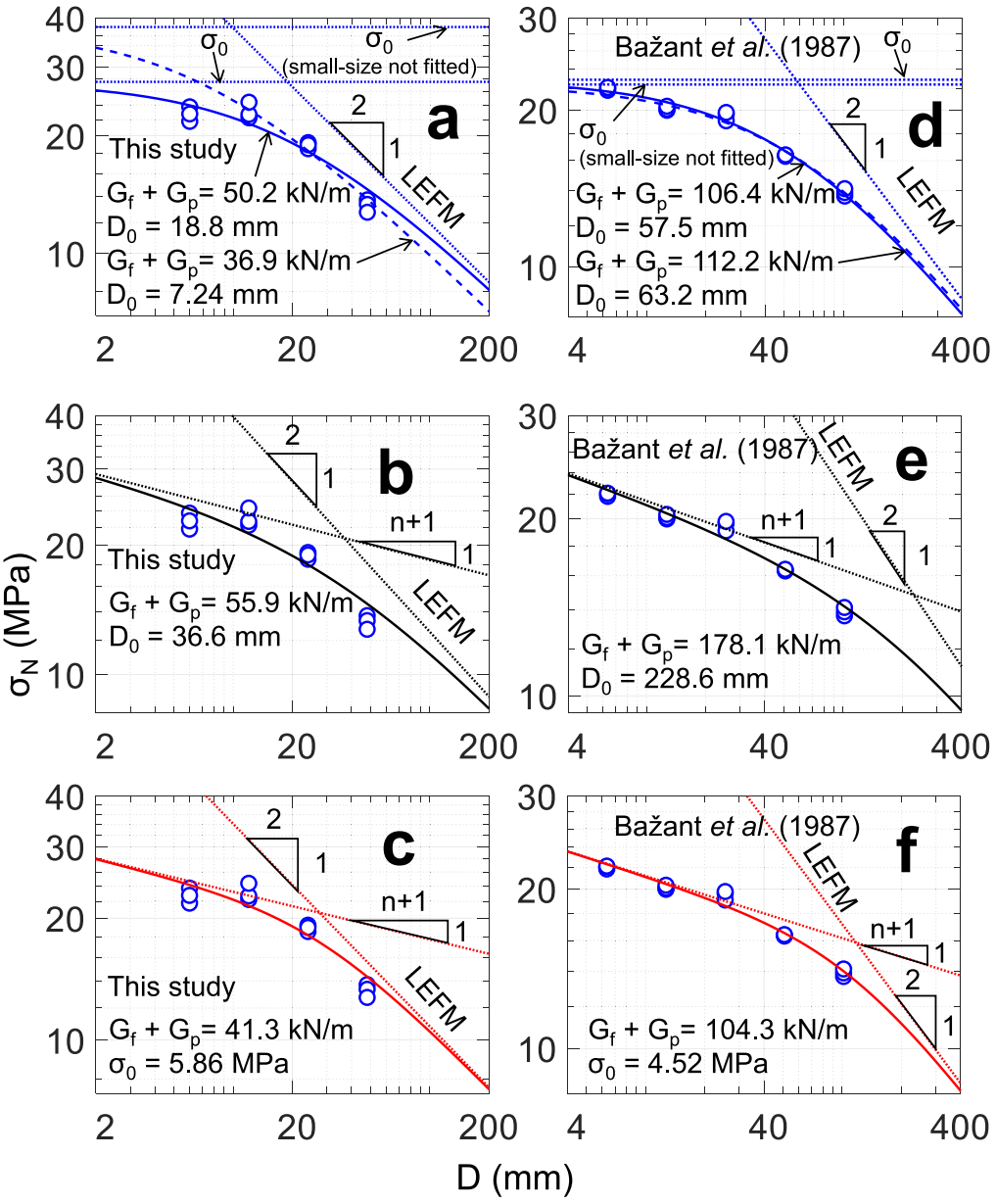

Fig. 5. Optimum fits of size effect law to test result on aluminum beams based on: (a,d) Eq. (53); (b,e) Eq. (57) (c,f). The transverse thickness of specimens was 10 mm (a,b,c), and 25.4 mm (1 in.) [30] (d,e,f).

If we substitute this equation, instead of Eq. (44), into the energy balance equation (43), we obtain, instead of Eq. (45), the following equation

$$\frac{\sigma_0^2}{E'}\left(\frac{\sigma_N}{\sigma_0}\right)^2 g_0 D + \frac{\sigma_0^2}{E'}\left(\frac{\sigma_N}{\sigma_0}\right)^{n+1} h_0 D = G_f + G_p \tag{57}$$

in which only the second term differs from Eq. (45). The above equation may be rewritten as

$$AX^{n+1} + BX^2 = C \qquad \text{in which} \tag{58}$$

$$A = (\sigma_0^2/E')h_0 D, \quad B = (\sigma_0^2/E')g_0 D,$$

$$C = G_f + G_p, \quad X = \sigma_N/\sigma_0 \tag{59}$$

It is necessary to acknowledge that Eq. (55) was previously obtained in a different way by Kanninen and Popelar [5, pp.c314–317]. They replaced the fixed limiting width of the yielding zone (here denoted as $2r_p$) by a reduced width restricted by the specimen size (Eqs. 5.4–9 and 5.4–11 in [5]). With their empirical function ϕ they achieved a smooth transition. For notched three-point bend specimens, they calculated by finite elements and tabulated a function, $h_1(\alpha, n)$, that describes this transition for various relative crack lengths α. The present constant h_0 may be taken as equal to $\alpha_p(1-\alpha)h_1(\alpha_0, n)$.

To obtain the size effect of D on σ_N, one needs to solve X as a function of A, B, C from Eq. (58). Since an exact solution is not possible for $n > 4$ (according to Abel–Galois theorem), a numerical solution is necessary but it may be easily obtained by Newton iterations or, more effectively, by minimizing the quadratic expression

$$\Phi = (AX^{n+1} + BX^2 - C)^2 \tag{60}$$

with an optimization algorithm such as Levenberg–Marquardt. Nevertheless, a very accurate closed-form analytical approximation is possible, as shown in the next section.

A tentative iterative procedure to identify the G_f and h_0 values from size effect tests may begin, in the first iteration, with a guess

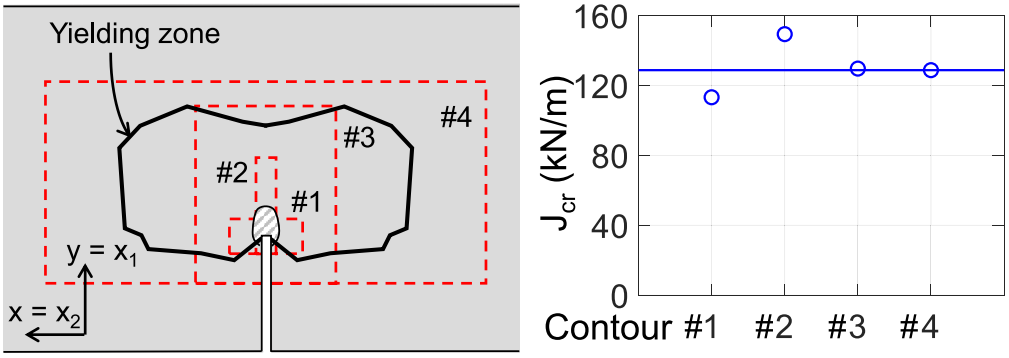

Fig. 6. J-integrals on different contours (the cross-hatched area indicates the fracture process zone, FPZ), computed on the specimens with $D = 24$ mm and transverse thickness $b = 25$ mm (Fig. 5d,e,f). Path 3 and 4 indicate path-independence, but 1 and 2 (which cross into the FPZ) do not.

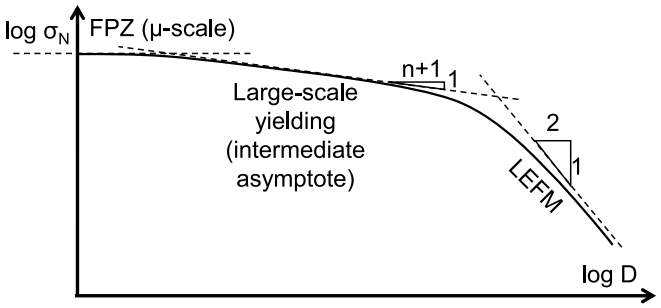

Fig. 7. Micron-scale asymptote for specimens with sizes comparable to process zone size (volume confined within slip planes or grain boundaries), and transition to intermediate asymptote and terminal asymptote.

of the values of $G_f + G_p$, σ_0 based on a preliminary estimate by linear regression according to Eq. (50). Minimization of Φ then yields the optimum values.

12. Closed-form approximation of small-to-large-scale yielding and evaluation of size effect tests

We denote:

$$X_A = (C/A)^{\frac{1}{n+1}}, \quad X_B = (C/B)^{\frac{1}{2}}, \quad Y = X/X_A, \quad m = X_A/X_B \tag{61}$$

by which Eq. (58) becomes

$$Y^{n+1} + m^2 Y^2 = 1 \quad \text{where} \quad m = \left(1 - Y^{n+1}\right)^{\frac{1}{2}}/Y \tag{62}$$

The real solution of this equation can be closely approximated by:

$$m = \left(Y^{-d} - 1\right)^{\frac{1}{d}} \quad \text{with} \quad d = \sqrt{2(n+1)} \tag{63}$$

and Y then follows from Eq. (61). Fig. 4 shows how close this approximation is. Note that this approximation does not depend on A, B and C. The maximum error occurs when $X \to X_A$ or $D \to 0$ but these are not realistic cases.

The ratio σ_N/σ_0 obtained from this solution converges to LEFM (though not SEL) as $n \to 1$. It may further be checked that $\sigma_N/\sigma_0 \to (kD/D_0)^{-\frac{1}{n+1}}$ for $D \to 0$, and $\sigma_N/\sigma_0 \to (D/D_0)^{-\frac{1}{2}}$ for $D \to \infty$.

Identification of fracture properties from size effect tests is done by directly optimizing σ_0 and $G_f + G_p$ based on Eq. (60). The standard algorithm for nonlinear optimization in commercial software, such as Matlab, can be used.

The optimum fits of the results of the present tests of geometrically scaled aluminum specimens are presented in Fig. Fig. 5a,b,c (for the details of the experiments, see section 14). They were obtained with Eqs. (46), (53) and (60). The transverse thickness of all specimens was not scaled and was kept as 10 mm. For comparison, the results of the tests performed on the same type of aluminum by Bažant, Lee and Pfeiffer [30] (in 1987, before the size effect theory was sufficiently developed) are also shown and analyzed; see Fig. 5d,e,f. The specimen dimensions in those tests were in the same range as here, except for the transverse thickness which was 25.4 mm (1 in.).

The plastic dissipation G_p can be calculated directly if one has the data from the standard uniaxial tensile test and if one determines the angular variations ψ_{ij} and φ_{ij} of stress and strain (which can be done, once for all, for any given specimen geometry, e.g., the 3PB test). If this is unavailable, one can obtain only the sum $G_f + G_p$ as a whole, which is what is done here.

Even though the values of $G_f + G_p$ of the tested material (Al 6061-T651) obtained from Eqs. (46), (53) and (60) were in a reasonable range, some discrepancies need to be noted. Eq. (53) tends to give a higher $G_f + G_p$ than the other two. Due to the assumption of a fixed r_p in Eq. (46), choosing the data points in which yielding zone is fully developed matters. This was reflected in Fig. 5a, in which the fitting of three larger sizes captured the data trend better and its resulting fracture energy was in agreement with Fig. 5c. So we consider this to be the true value of $G_f + G_p$. The same conclusion can be drawn from Fig. 5d,f. In this case, however, including or excluding the anomalous test result from the smallest specimen did not make a big difference.

According to [41], the transverse thickness has an appreciable effect. In large-scale yielding, the material at mid-thickness will begin yielding first. Because the material on the sides has not yet yielded, a plane-strain constraint develops at the middle part of the crack front edge, which creates a triaxial stress state. The larger the transverse thickness, the stronger the plane strain effect. This tends to increase $G_f + G_p$. Further tests are necessary to assess the magnitude of this effect as an envelope of fracture equilibrium curves.

The standard ASTM-E1820 [42] provides a guideline to measure the fracture energy of plastic-hardening materials. This includes the procedures for (a) the basic test of J_{Ic} and (b) the resistance curve (R-curve). The former requires a number of identical specimens to be loaded to different load levels, with several load–displacement curves to be recorded. This results in a J–Δa curve, based on which the J_{Ic} is obtained by interpolation. The latter method, on the other hand, demands only one specimen, but the loading procedure include multiple loading–unloading cycles to keep track of the structure compliance. The proposed method which requires testing only the maximum loads of geometrically-scaled specimens of at least three different sizes seems relatively simpler. It is also related to the R-curve method, as documented

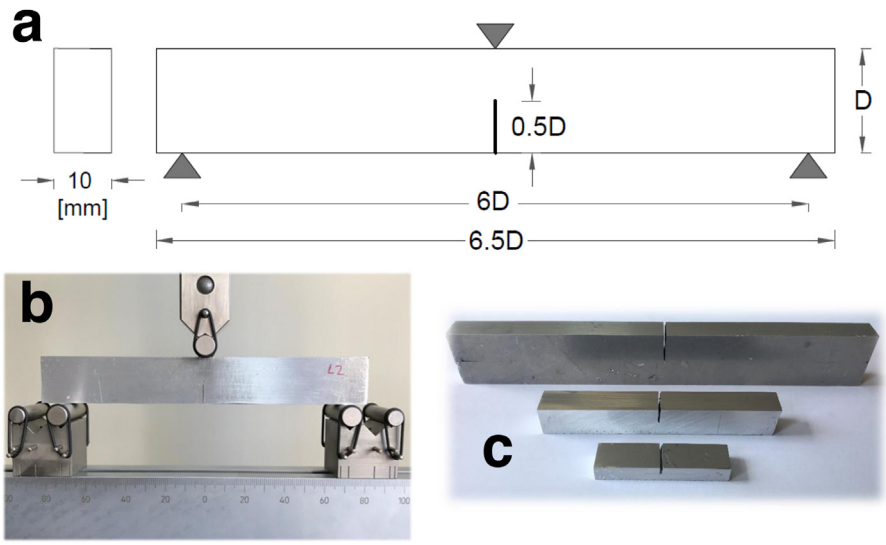

Fig. 8. (a) Schematic and (b) actual setup of notched three-point-bend tests; (c) Geometrically-scaled specimens with the same transverse thickness and various depths, $D = 6, 12, 24$ mm (specimens with $D = 48$ mm were tested but not shown here).

in 1967 in [30] where the way to calculate the R-curve from the size-effect was shown.

To confirm the validity of the present method, finite element simulations of the tested material have been performed using a well established material model for the metals presented in [43,44]. Calibrating the material model with uniaxial tensile test data and the load–displacement curve of a specimens of one depth ($D = 24$ mm), J-integral calculations were run for various contours.

After calibration, J-integral calculations were run for various contours. It is important to choose contours for which the J-integral is path-independent. They are those on which there is no unloading. For the contours in Fig. 6, if the contour crosses the plastically unloaded region or the damage region of the FPZ (e.g. 1 and 2), the calculated J-integral will be path-dependent. However, if the contour passes entirely through the HRR field, and not the FPZ, its J-integral will be path-independent and will be the same as for a contour lying outside both zones. It is this value that is selected as the correct J_{Ic} of the material. This J_{Ic} (128.4 kN/m) differs by 16% from the J_{Ic} value obtained using size effect method (112.2 kN/m).

13. Scaling for the FPZ-to-yielding transition and intermediate asymptote

When the specimen becomes smaller than the FPZ, which has a size in the micrometer range, the scaling is that of damage mechanics and is the same as for quasibrittle materials. Based on what is known for these materials [20,45], the approach of the size effect curve to zero size must be linear. This translates, in the log–log scale, to an exponential, with a horizontal asymptote in that scale.

When the specimen becomes much larger than the FPZ but still significantly smaller than the yielding zone which (being of millimeter dimensions) is three order of magnitude larger, the large-size asymptote must be of the type $D^{-\frac{1}{n+1}}$. The simplest asymptotic matching formula then is

$$\sigma_N = \sigma_1 \left(1 + \frac{D}{D_1}\right)^{-\frac{1}{n+1}} \tag{64}$$

where σ_1 and D_1 are constants. This equation is valid only when D is smaller by at least one order of magnitude than the yielding zone size.

Considering the full size range from the FPZ to the specimen much larger than the yielding zone, we thus have three asymptotic regimes:

$$\sigma_N \propto D^0, \quad D^{-\frac{1}{n+1}}, \quad D^{-\frac{1}{2}} \tag{65}$$

The second is what Barenblatt named, and rigorously defined, as the intermediate asymptote [46] (Fig. 7). The intermediate asymptote $D^{-\frac{1}{n+1}}$ serves both as the large-size asymptote for the FPZ-to-yielding transition and as the small-size asymptote for the yielding-to-elasticity transition.

14. Tests of notched specimens of aluminum and comparisons

A total of 12 notched three-point-bend (3PB) fracture specimens of aluminum (of type Al 6061-T651) have been manufactured (Fig. 8). The experiments involved 4 different sizes with the size range of 1 : 2 : 4 : 8. Three identical specimens were tested for each size. The span-to-depth ratio was 6.0 and the relative notch depth was $a/D = 0.5$. The specimens of all sizes and their notches were geometrically similar in two dimensions but the transverse thickness, $b = 10$ mm, was kept constant (in order to avoid having to separate the size effects of plastic shear lip and of 3D singularity of stress field at the intersections of the crack front edge with the side faces).

The tests have been conducted in a MTS servo-controlled testing machine with load capacity of 10 kN and digital closed-loop controls. The built-in three-point-bend fixture of the system has been used as the test setup. Steel rollers have been placed at the load point and at end supports. The built-in load-cell and linear variable differential transformer (LVDT) have been employed and calibrated before testing. Displacement controlled loading was used. The loading rate was 0.002 mm/s for the smallest-size specimens. For larger sizes, the loading rate has been scaled so as to keep the strain rate approximately the same for all the sizes. The loading continued into the postpeak until the load dropped to 80% of the peak load.

Similar tests of aluminum have been conducted already in 1987 by Bažant, Lee and Pfeiffer [30], before the size effect theory was fully developed. Fig. 8 demonstrates that the size effect derived here matches these tests quite well.

15. Conclusions

1. In contrast to quasibrittle fracture, the analysis of ductile fracture of plastic-hardening materials is complicated by the existence of a millimeter-scale yielding zone separating the unloading elastic zone of structure from the micrometer-scale damage zone of fracture process.
2. The effective size of the yielding zone is properly determined by using the principal of virtual work to enforce equilibrium in the zone of transition between the plastic hardening zone and elastic zone. Alternatively, the same effective size is obtained by minimizing the squared difference of these fields integrated over this zone. This furnishes the yielding zone size as a function of the crack-parallel T-stress.
3. In addition to the energy released from the structure, further energy is released from the unloaded band of material trailing the advancing yielding zone. In addition to the energy dissipated at fracture front, further energy is dissipated by irreversible unloading of the material behind the advancing yielding zone. The energy flux described by the J-integral delivers energy through the yielding zone to the fracture process zone at crack front, but neither releases nor dissipates any energy within the yielding zone.
4. Balance of energy release and energy dissipation leads to an approximate size effect law for plastic-hardening fracture matching the asymptotic behaviors on both sides of the size scale. The law is of the same form as the classical size effect law (of Type 2) for quasibrittle materials such a concrete. However, the coefficients in this law are related to the material properties in a different way.
5. Based on the size effect law derived, the identification of fracture energy and effective size of the yielding zone for specimens significantly larger than the yielding zone is reducible to linear regression.
6. When the test data range reaches into specimens so small that the development of the crack tip yielding zone is restricted by the boundaries, a modification of the size effect law is required. Linear regression is then impossible but identification of fracture properties is still possible.
7. The derived size effect law is verified by two series of tests of scaled notched three-point bend specimens of aluminum.
8. The size effect method is a relatively simple method to estimate the fracture energy of plastic-hardening materials. It is simpler than the elaborate procedure specified in ASTM-E1820 [42]. However, broader experimental verification is appropriate and some details might still need to be worked out.

Declaration of competing interest

The authors declare that they have no known competing financial interests or personal relationships that could have appeared to influence the work reported in this paper.

Acknowledgments

Financial support under National Science Foundation Grant CMMI-2029641 to Northwestern University is gratefully acknowledged. A.A.D. thanks Istanbul Technical University for further financial support.

Appendix A. J-Integral evaluation

Substituting Eqs. (18), (19), (20) and (36) in Eq. (14) and integrating on the circular contour of radius r_p, one finds that

$$J = 1/2\alpha_p \epsilon_y \sigma_y c_J, \quad \text{where:} \tag{66}$$

$$c_J = \int_{-\pi}^{\pi} \left[\frac{n\varphi_{ij}(\theta)}{n+1} - \frac{\nu_j F_i(\theta)}{n+1} + \nu_j F_i'(\theta) \tan^2\theta \right] \psi_{ij}(\theta) \cos\theta \left(\frac{\sigma_N}{\sigma_0} \right)^{n+1} h_0 D \, \mathrm{d}\theta \tag{67}$$

Appendix B. Generalized estimates of energy matching zone radius r_p'

Eq. (31) for estimating r_p and r_p' depends on calculating the virtual work only for strain component $\delta\epsilon_{xx}$ (or $\delta\epsilon_{11}$), which is in the crack direction. But one could, of course, calculate the virtual work for other components, and in each case one would get a different result for r_p'. But they would all have the same form as Eq. (31) except that factor C_e and C_p would have different values (while C_n not).

Still another way is to impose the virtual work equivalence required for overall equilibrium (or alternatively least-square match) for any direction θ characterized by unit vector ν_i in direction θ, replace $\delta\epsilon_{11}$ by $\delta\epsilon_{ij}$ [23–27], and use resultants $\nu_j s_{ij}$ and $\nu_j e_{ij}$ to replace s_{11} and e_{11} in Eq. (29). The result will have the same form as (31) but with different coefficients depending on θ. Averaging over θ would give a single prefactor value. This again shows that C_e, C_p, as well as parameter $\zeta = r_p'/r_p$, is only a crude estimate, and FE analysis would be needed for more accurate results.

It is, however, important to mention that the prefactor values delivered by various ways of calculating C_e and C_p do not differ much. Therefore, such a degree of uncertainly is not important for a scaling law spanning 8 orders of magnitude, from 10^{-7} m (a grain within the micrometer size FPZ) to 10 m (large structure size).

More generally, to represent the case of plane strain, the crack-parallel stress $\sigma_{11} = T$ is accompanied by out-of-plane $\sigma_{33} = \nu T$. Then, instead of Eq. (28), the full first two terms in the LEFM near-tip asymptotic series expansion read [36]:

$$\sigma_{ij} = \frac{K_I}{\sqrt{r}} f_{ij}(\theta) + T\delta_{1i}\delta_{j1} + k_\epsilon \nu T \delta_{3i}\delta_{j3} \tag{68}$$

where $k_\epsilon = 0$ for plane stress and $k_\epsilon = 1$ for plane strain.

In general three-dimensional situations, one may have to generalize Eq. (68) by considering in the crack-parallel plane (x, z) a general stress state, i.e. T_{xx}, T_{zz}, T_{xz}. By experience with concrete, T_{zz} may be as important as $T = T_{xx}$.

References

[1] J.W. Hutchinson, Singular behaviour at the end of a tensile crack in a hardening material, J. Mech. Phys. Solids 16 (1) (1968) 13–31.
[2] J. Rice, G.F. Rosengren, Plane strain deformation near a crack tip in a power-law hardening material, J. Mech. Phys. Solids 16 (1) (1968) 1–12.
[3] J.R. Rice, A path independent integral and the approximate analysis of strain concentration by notches and cracks, ASME J. Appl. Mech. 35 (2) (1968) 379–386.
[4] T.L. Anderson, Fracture Mechanics: Fundamentals and Applications, CRC Press, Boca Raton, FL, 1991.
[5] M.F. Kanninen, C.H. Popelar, Advanced Fracture Mechanics, in: Oxford engineering science series, Oxford University Press, New York, 1985.
[6] N.P. O'dowd, C.F. Shih, Family of crack-tip fields characterized by a triaxiality parameter—I. Structure of fields, J. Mech. Phys. Solids 39 (8) (1991) 989–1015.
[7] N.P. O'Dowd, C.F. Shih, Family of crack-tip fields characterized by a triaxiality parameter—II. Fracture applications, J. Mech. Phys. Solids 40 (5) (1992) 939–963.

[8] C. Betegón, J.W. Hancock, Two-parameter characterization of elastic-plastic crack-tip fields, J. Appl. Mech. 58 (1) (1991) 104–110.
[9] L. Xia, T. Wang, C. Shih, Higher-order analysis of crack tip fields in elastic power-law hardening materials, J. Mech. Phys. Solids 41 (4) (1993) 665–687.
[10] X. Gao, C. Shih, V. Tvergaard, A. Needleman, Constraint effects on the ductile-brittle transition in small scale yielding, J. Mech. Phys. Solids. 44 (8) (1996) 1255–1282.
[11] Hoang Nguyen, M. Pathirage, M. Rezaei, M. Issa, G. Cusatis, Z.P. Bažant, New perspective of fracture mechanics inspired by gap test with crack-parallel compression, Proc. Natl. Acad. Sci. 117 (25) (2020) 14015–14020.
[12] Hoang Nguyen, M. Pathirage, G. Cusatis, Z.P. Bažant, Gap test of crack-parallel stress effect on quasibrittle fracture and its consequences, J. Appl. Mech. 87 (7) (2020).
[13] E.O. Hall, The deformation and ageing of mild steel: III discussion of results, Proc. Phys. Soc. B 64 (9) (1951) 747.
[14] A.H. Cottrell, Dislocations and Plastic Flow in Crystals, Oxford University Press, 1958.
[15] J.R. Greer, J.Th.M. De Hosson, Plasticity in small-sized metallic systems: Intrinsic versus extrinsic size effect, Prog. Mater. Sci. 56 (6) (2011) 654–724.
[16] D. Kiener, W. Grosinger, G. Dehm, R. Pippan, A further step towards an understanding of size-dependent crystal plasticity: In situ tension experiments of miniaturized single-crystal copper samples, Acta Mater. 56 (3) (2008) 580–592.
[17] M.C. Shaw, The size effect in metal cutting, Sadhana 28 (5) (2003) 875–896.
[18] Z.P. Bažant, J.L. Le, Probabilistic Mechanics of Quasibrittle Structures, Cambridge University Press, 2017.
[19] Z.P. Bažant, E.-P. Chen, Scaling of structural failure, Appl. Mech. Rev. ASME 50 (10) (1997) 593–627.
[20] Z.P. Bažant, Scaling of Structural Strength, second ed., Elsevier Science, 2005.
[21] W. Ramberg, W.R. Osgood, Description of Stress-Strain Curves by Three Parameters, Technical Note 902, NACA, Washington, D.C., 1943.
[22] J.W. Hutchinson, P.C. Paris, Stability analysis of J-controlled crack growth, in: Elastic-Plastic Fracture, ASTM International, 1979.
[23] J.R. Rice, Mathematical analysis in the mechanics of fracture, Fract.: Adv. Treatise 2 (1968) 191–311.
[24] G.P. Nikishkov, J-A fracture concept based on the three-term elastic-plastic asymptotic expansion of the near-crack tip stress field, in: Fracture: A Topical Encyclopedia of Current Knowledge, Citeseer, 1998, pp. 557–574.
[25] B. Revil-Baudard, O. Cazacu, N. Chandola, Effect of the yield stresses in uniaxial tension and pure shear on the size of the plastic zone near a crack, Int. J. Plast. 102 (2018) 101–117.
[26] G. Xin, W. Hangong, K. Xingwu, J. Liangzhou, Analytic solutions to crack tip plastic zone under various loading conditions, Eur. J. Mech. A Solids 29 (4) (2010) 738–745.
[27] N. Levy, P.V. Marcal, W.J. Ostergren, J.R. Rice, Small scale yielding near a crack in plane strain: a finite element analysis, Int. J. Fract. Mech. 7 (2) (1971) 143–156.
[28] J.W. Hutchinson, Plastic stress and strain fields at a crack tip, J. Mech. Phys. Solids 16 (5) (1968) 337–342.
[29] Z.P. Bažant, Size effect in blunt fracture: concrete, rock, metal, J. Eng. Mech. 110 (4) (1984) 518–535.
[30] Z.P. Bažant, S.-G. Lee, P.A. Pfeiffer, Size effect tests and fracture characteristics of aluminum, Eng. Fract. Mech. 26 (1) (1987) 45–57.
[31] Z.P. Bažant, M.T. Kazemi, Size effect on diagonal shear failure of beams without stirrups, ACI Struct. J. 88 (3) (1991) 268–276.
[32] Z.P. Bažant, J. Planas, Fracture and Size Effect in Concrete and Other Quasibrittle Materials, in: New Directions in Civil Engineering, CRC Press, Boca Raton and New York, 1998.
[33] G. Cusatis, E.A. Schauffert, Cohesive crack analysis of size effect, Eng. Fract. Mech. 76 (14) (2011) 2163–2173.
[34] Z.P. Bažant, Q. Yu, Size-effect testing of cohesive fracture parameters and non-uniqueness of work-of-fracture method, ASCE J. Eng. Mech. 137 (8) (2011) 580–588.
[35] RILEM Recommendation TC89-FMT, Size-effect method for determining fracture energy and process zone size of concrete, Mater. Struct. 23 (6) (1990) 461–465.
[36] M.L. Williams, Stress singularities resulting from various boundary conditions in angular corners of plates in extension, J. Appl. Mech. 19 (4) (1952) 526–528.
[37] C.F. Shih, J.W. Hutchinson, Fully plastic solutions and large scale yielding estimates for plane stress crack problems, J. Eng. Mater. Technol. 98 (1976) 289–295.
[38] G. Herrmann, H. Sosa, On bars with cracks, Eng. Fract. Mech. 24 (6) (1986) 889–894.
[39] R. Kienzler, G. Herrmann, An elementary theory of defective beams, Acta Mech. 62 (1–4) (1986) 37–46.
[40] Z.P. Bažant, L. Cedolin, Stability of Structures: Elastic, Inelastic, Fracture, and Damage Theories, in: Oxford Engineering Science Series, Oxford University Press, 1991.
[41] R. Narasimhan, A.J. Rosakis, Three-dimensional effects near a crack tip in a ductile three-point bend specimen: Part I—A numerical investigation, J. Appl. Mech. 57 (3) (1990) 607–617.
[42] American Society for Testing and Materials, Standard Test Method for Measurement of Fracture Toughness, ASTM International, West Conshohocken, PA, 2020.
[43] A. Srivastava, L. Ponson, S. Osovski, E. Bouchaud, V. Tvergaard, A. Needleman, Effect of inclusion density on ductile fracture toughness and roughness, J. Mech. Phys. Solids 63 (2014) 62–79.
[44] K.K. Mathur, A. Needleman, V. Tvergaard, Three dimensional analysis of dynamic ductile crack growth in a thin plate, J. Mech. Phys. Solids 44 (3) (1996) 439–464.
[45] Z.P. Bažant, Scaling theory for quasibrittle structural failure, Proc. Natl. Acad. Sci. 101 (37) (2004) 13400–13407.
[46] G.I. Barenblatt, Similarity, Self-similarity, and Intermediate Asymptotics, Consultants Bureau, New York, 1979.